Final Report

Submitted to

National Aeronautics and Space Administration
Mission to Planet Earth
Science Division
Code YS

on

Grant NAG11831

Entitled:

Development of Corrections for Biomass Burning Effects in Version 2 of GEWEX/SRB Algorithm

Report Period: 07/01/1996-12/31/1999

Submitted by:

Rachel T. Pinker, PI.

and

I. Laszlo, Co-PI

Department of Meteorology
University of Maryland
College Park, Maryland 20742

Tel: 301-405-5380
Fax: 314-9482
e-mail: pinker@atmos.umd.edu

Table of Content

Objectives

The objectives of this project were:

- To incorporate into an existing version of the University of Maryland Surface Radiation Budget (SRB) model, optical parameters of forest fire aerosols, using best available information, as well as optical properties of other aerosols, identified as significant.

- To run the model on regional scales with the new parametrization and information on forest fire occurrence and plume advection, as available from NASA LaRC, and test improvements in inferring surface fluxes against daily values of measured fluxes.

- Develop strategy how to incorporate the new parametrization on global scale and how to transfer modified model to NASA LaRC.

Relevance of topic

Monitoring and predicting effects of radiatively important trace gases, have been important issues in climate research. Many studies have been undertaken to predict possible climate changes, in particular, changes in surface temperature, due to different scenarios of CO2 concentrations, such as doubling of its content in the atmosphere. As yet, the CO2 budget in the atmosphere is not fully understood (Keeling et al., 1995), and even less is known how it affects the global radiation budget(Penner et al., 1992).

The effects of atmospheric aerosol particles added as a result of biomass burning, have not been fully evaluated, and are difficult to model because of their relatively short lifetimes and irregular spatial distribution. The global mass of smoke in the atmosphere depends on the total rate of biomass burning, the fraction of burned material that goes into smoke, and the lifetime of the smoke in the atmosphere (Penner et al., 1992). More than 70% of the burned biomass is in the tropics, and savannas play a dominant role (Seiler and Crutzen, 1980), and the estimated production is believed to be comparable to the global annual anthropogenic sulfate production (Charlson et al., 1991). The smoke has similar distribution of particle sizes as sulfate aerosols, and they include hygroscopic components. The optical thickness is determined by the absorption and scattering optical depths. Information on aerosol properties of smoke for different types of forest fires have been estimated (Radke et al., 1988; Ferrare et al., 1990). These estimates suggest values of 0.85 to 0.90 for the single scattering albedo, $\acute{\omega}_0$, of dry smoke, and 0.90 to 0.95 for aerosols that have absorbed

ambient water molecules. Aerosols that become cloud condensation nuclei will change the radiative properties of clouds; this will lead to a modified top of the atmosphere albedo (Twomey, 1971), and consequently, alter the estimates of the surface radiation budget.

Under this project it was planned to evaluate the effects of aerosols (e. g., forest fires and dust)and their optical properties on the SRB inference methods. This is now feasible due to progress made in building data bases on biomass burning and co-located surface measurements (e. g., Cahoon et al., 1992). Information on the optical properties of soot, as well as on dust and sulfate aerosols, is also available. Numerous sources can be found in d'Almeida, Koepke and Shettle (1991). They also propose detailed models of different aerosol types. For carbonaceous substances they compiled information on the refractive indices, and distinct between graphite, coal, and soot (Rosen and Novakov, 1984; Twitty and Weinman, 1971). According to Charlson et al. (1987), tropical vegetation and soil, specifically during the rainy season, are strong sources of gaseous compounds of sulfur. The amount of cloud condensation nuclei will increase with the number of concentration of sulfate particles. Arid and semi-arid regions that are a major source of dust aerosols, cover a third of the earth's surface, and are therefore important in modeling radiative transfer in the atmosphere. Information on source strength and optical properties of such aerosols have been made by numerous investigators (Schutz and Jaenicke, 1974; d'Almeida and Schutz, 1983; d'Almeida, 1986; Patterson and Gillette, 1977; Ackerman and Cox, 1982). These studies were utilized by d'Almeida et al. (1991), to propose a characteristic desert aerosol model.

The work done under this proposal is strongly linked to our past and ongoing activity on the development and implementation of methodologies to derive surface and top of the atmosphere shortwave radiative fluxes from satellite observations. The goal is to bring updated model versions into an operational status at NASA LaRC. Working procedures have been developed between the University of Maryland and the NASA Langley Research Center that enable smooth transfer of models.

1. Relevant results from prior research

1.1 Background

The primary objectives of past activities in the area of surface radiation budgets (SRB) by methods of remote sensing, were: to develop, validate and implement methods to derive large scale surface and top of the atmosphere shortwave radiation budgets. This objective has been accomplished, and a working algorithm has been provided to

NASA LaRc for implementation on global scale. Global scale validation was undertaken at NASA LaRC, using SRB values as derived independently at LaRC, and ground truth as available from the Global Energy Budget Archive (GEBA), World Radiation Data Center, Zurich, Switzerland. The primary source of satellite data used for methodology implementation were those developed under the International Satellite Cloud Climatology Project (ISCCP) (Schiffer and Rossow, 1985; Rossow and Schiffer, 1991). The validation effort of the inferred surface fluxes has shown, that on the average, the accuracies required by climate models can be reached. Closer examination of cases during periods of biomass burning, primarily in Africa and South America, have indicated that the inferred values are less accurate than the one obtained during periods of no biomass activity. At present, it is not clear if the cause of these differences is related to the satellite data provided as input to the inference models, or due to the use of aerosol and cloud absorption parametrizations, that do not represent such events. Since our SRB activity was initiated, there have been new developments, that will allow to examine these issues more closely. Information on the occurance of biomass burning is becoming available on global scale from the DMSP and AVHRR sensors. Ground truth on a daily time scale has been prepared at the World Radiation Data Center, St. Petersburg, Russia.

Direct biomass burning effects on satellite estimates of shortwave surface radiation in Africa, have been investigated by Whitlock et al. (1995). It is claimed that it is possible to detect the effects of biomass burning on the accuracy of the derived surface fluxes, when compared with accuracies during low biomass burning periods. Therefore, regions in Africa where both effects occur (biomass burning and dust episodes), are most appropriate for testing possible improvements in the inference methods.

The current version of our SRB inference model allows clouds to be placed at different vertical levels, and to include different parametrizations of cloud optical properties. Therefore, it can be implemented with improved characterization of different cloud types (e. g., cirrus), or specific aerosol types (e. g., soot from forest fires). These capabilities of the model were used to learn if improvements can be achieved in predicting surface fluxes, by incorporating latest information on the distribution of biomass burning locations and optical parameters of aerosols that play a role during biomass burning episodes (e. g., soot; sulfates; dust).

1.2 Issues

The surface fluxes estimated by the Global Energy and Water Cycle Experiment, Surface Radiation Budget (GEWEX/SRB)

shortwave algorithm (Pinker and Laszlo, 1992) include the effect of varying amount of aerosols on radiation. This effect is calculated by estimating the amount of aerosols from satellite-observed clear-sky radiances, a time-history of the clear-sky radiances, and climatology of the aerosol loading used for initialization. In the process, models are used to describe the radiative properties and vertical distribution of aerosols. In Version 1 of the algorithm, the aerosol climatology used for initialization was limited. The aerosol optical depth depended only on a few surface types (water, land, desert and snow), and radiative properties were modeled using the continental and maritime models of the Standard Radiation Atmospheres (SRA; WCP-55, 1983). A comparison of satellite-based estimates of shortwave surface radiative fluxes with ground-based observations showed that the satellite-estimated fluxes were less accurate in regions of intense biomass burning and heavy aerosol concentrations. Aerosols emitted by fires were suspected to cause these differences because the satellite reduction algorithm does not explicitly account for them (Konzelmann et al., 1996).

To better represent the radiative effects of aerosols,

- a spatially and temporally detailed aerosol climatology is needed;
- the spatial and temporal extent of episodic biomass burning must be identified;
- models describing the optical properties and vertical profiles of various aerosol mixtures found in the atmosphere must be built.

We have evaluated two aerosol climatologies: maps of aerosol optical depths derived from chemical transport models, and as obtained from surface aerosol optical depth measurements. To consider the effect of aerosols released during biomass burning episodes, aerosol models appropriate for smoke were built into the GEWEX/SRB algorithm, and the location and extent of biomass burning were identified from smoke maps generated by chemical transport models. Surface fluxes were derived from the algorithm using the new aerosol models, and the results were compared to observations. Details are given below.

2. Accomplishments

2.1 Models of biomass-burning aerosols

Microphysical properties of biomass burning aerosols were modeled following Liousee et al. (1997). Two models (Types 1 and 2) were constructed by externally mixing organic carbon, black carbon, dust and water-soluble particles of different mean radii and volume concentrations. Particle

size was assumed to vary according to a lognormal distribution (Table 1 and Figure 1). Type-1 model is assumed to model "young" plumes with particles of small geometric mean radii, while Type-2 model with larger radii is intended to model "old" smoke plumes carried by the wind far from their origin. Optical parameters for these models were obtained from standard Mie calculations assuming spherical shape of particles (Figure 2). Vertical profiles were set up combining the profiles in Anderson et al. (1996) and WCP-55 (1983). The profiles for Type-1 and Type-2 aerosols are shown in Figure 3, along with the profiles in the Standard Radiation Atmospheres, SRA (WCP-55, 1983).

Table 1. Carbonaceous Aerosol Models

Component	r_v (μm)	r_g (μm)	σ	m	V_i (%)
		Type 1			
Organic carbon	0.03	0.015	1.70	1.43-0.0035i	81.4
Black carbon	0.04	0.015	1.70	1.95-0.6600i	12.0
Dust-like	12.20	2.300	2.11	1.50-0.0008i	4.9
Water-soluble	0.18	0.005	2.99	1.53-0.005i	1.7
		Type 2			
Organic carbon	0.10	0.040	1.70	1.43-0.0035i	87.0
Black carbon	0.80	0.200	2.00	1.95-0.6600i	11.0
Dust-like	12.20	2.300	2.11	1.50-0.0008i	0.5
Water-soluble	0.80	0.200	2.00	$1.53-10^{-7}i$	1.5

Lognormal size distribution was used; r_v: volume mean radius; r_g: geometric mean radius; σ_g: geometric standard deviation, m: complex refractive index; V_i: volume concentration.

In a 2.5x2.5 deg grid used by ISCCP, one will rarely observe only a single profile; instead, the mean radiance representing such a scale will correspond to a mixture of smoke and "background" profiles. In addition, on the monthly time scales available from current aerosol climatologies, "old" smoke will likely dominate the scene. Therefore, the smoke profiles and SRA profiles were weighted in the final aerosol model (BMB according to the following formula:

Over land:

$$K(0\text{-}2\ \text{km}) = 0.5\ K_{\text{Cont-I}} + 0.5\ K_{\text{Type-1}}$$
$$K(2\text{-}4\ \text{km}) = 0.2\ K_{\text{Cont-I}} + 0.1\ K_{\text{Type-1}} + 0.7\ K_{\text{Type-2}}$$

Over ocean:

$$K(0\text{-}2\ \text{km}) = K_{\text{Mar-I}}$$
$$K(2\text{-}4\ \text{km}) = 0.3\ K_{\text{Mar-I}} + 0.05\ K_{\text{Type-1}} + 0.65\ K_{\text{Type-2}}$$

Above four kilometers, the profiles are the same as those in the standard SRA models. In the formulas above, K is substituted for any of the optical parameters. The weighted profiles are shown in Figure 4. Reflectances and

transmittances were calculated with these aerosols, and added to the look-up tables used by the GEWEX/SRB algorithm.

Ideally, information on aerosol should be on the same spatial and temporal scales as those of the satellite data used for estimating the SW irradiance. Such information, however, is currently not available on a global scale. Therefore, we have experimented with two alternatives:

- Aerosol climatology derived from chemical transport models. The advantages of such climatology are global coverage and some spatial and temporal detail. However, this type of climatology usually provides only total particulate matter that needs to be converted into optical depth. In addition, because of the uncertainties involved in the global sources, the resulting aerosol amounts and consequently the optical depths require some "tuning".

- Aerosol climatology obtained from surface optical depth measurements. This type of climatology is not available globally.

Both types of climatologies are currently available only on a monthly time scale; which might make them inappropriate for retrievals of surface fluxes at higher time resolutions.

2.2 Aerosol climatology from Global Chemical Transport Models

Temporal and spatial extent of smoke was identified from the monthly smoke-plume map obtained from the NOAA/GFDL (National Oceanic and Atmospheric Administration Geophysical Fluid Dynamics Laboratory) Global Chemical Transport Model (GCTM). The GCTM uses estimates of biomass burning emissions, climatological total annual emissions, and climatological transport to produce monthly averages of total particulate matter (TPM) from fires. Digital smoke data containing TPM emissions from fires in Africa were obtained from the GCTM (P. Stackhouse, J. Olson and D. Cahoon (private communication). First, the data were re-gridded from the 2.4x2.4-degree grid to a 2.5x2.5 degree latitude/longitude grid; and then remapped to an equal-area grid to be used in the SRB algorithm with the ISCCP D1 data. The TPM values were converted into optical depth values using specific mass extinction cross-sections from Liousee et al. (1997) and Anderson et al. (1996), and using the relationship $\tau=\beta_s$ TPM, where τ is the aerosol optical depth, and β_s is the specific mass extinction cross-section. It is well known that different combustion fuels (differences in vegetation) produce different types of combustion products. Because of this, the conversion from TPM to aerosol optical depth is expected to be different for different regions. In

the experiments described below, total particulate matter was converted into initial optical depth values assuming two different values of the specific extinction cross-section. An example of the optical thickness field for June 1986 in Africa is shown in the top panel of Figure 5.

To describe a more detailed geographical distribution and seasonal variation of the aerosol loading the monthly aerosol-optical-depth maps of Tegen et al. (1997) were introduced to initialize the optical depth field in the retrieval of shortwave fluxes. In these maps, global distributions of aerosol loading resulting from transport models for soil dust, sulfate, sea salt, and carbonaceous aerosol are combined. The data were remapped from the original 2x4 deg horizontal resolution (GISS GCM format) to the 2.5x.2.5 deg grid used by ISCCP; and column optical depth were calculated by summing up the optical depths of individual aerosol components. The resulting total column optical thickness is smaller than that from the SRA for most areas for June (the month used in this study), except for the Amazon Basin, Eastern Europe, Russia, off the coast of Angola, Ethiopia, India, and Northern China (Figure 6).

2.3 Aerosol climatology from surface measurements

2.3.1 Clear-sky transmittances

Aerosol optical depths were obtained from the monthly clear-sky transmittances of DiPasquale et al. [1996]. The clear-sky transmittances were available for several hundred locations, and they were obtained by combining surface downward fluxes available from the WCRP archive (Ohmura and Gilgen, 1991), top of atmosphere downward irradiance, and ISCCP-estimated cloud cover. The aerosol optical depths were obtained from the transmittances applying the same radiative transfer package as used in the GEWEX/SRB algorithm. Software was written to supply the necessary input (transmittance, ozone and water vapor amounts, and surface albedo) for the radiative transfer package, and to invert the transmittance to obtain optical depth. Ozone and water vapor amounts were supplied from the ISCCP D1 data. The derived optical depth is shown in Figure 7. It must be noted, however, that the only about 15% of the clear-sky transmittances used in determining the aerosol optical depth were from scenes with zero (ISCCP-determined) cloud cover (see Figure 8). Many of he aerosol optical depth values, therefore, are likely being overestimated.

2.3.2 Aerosol optical depths

In December of 1996, a CIMEL sunphotometer was installed at the USDA-Agricultural Research Service Walnut Gulch Experimental Watershed, Arizona, to provide information on aerosol optical depths and other aerosol optical parameters

(Figure 4). This instrument is an automatic sun-tracking sky radiometer capable of measuring both sun and sky radiance, and by using a combination of spectral filters and azimuth/zenith viewing controlled by a microprocessor, enables to derive aerosol properties, total column water vapor and ozone. The CIMEL instrument was operated in the framework of the Aerosol Robotic Network (AERONET) that was established to obtain coherent observations of aerosol optical properties at various locations over the globe, in support of NASA's Earth Observing System (EOS) program. The data are transmitted via the GOES satellite to Goddard Space Flight Center, where they are centrally archived, and pre-processed (Holben et al., 1998). We have subjected the data to additional quality control, and the monthly mean values of aerosol optical depth used in this study are presented in Table 2. The Walnut Gulch was selected for the aerosol measurements to avoid urban influences, and because personnel was available at the site. Surface radiation measurements from the closest AZMET station (Tucson, AZ) were used. This data set was used to test the sensitivity of a radiation inference scheme to aerosols, in particular, on the determination of clear sky fluxes and the surface albedo. More details on the measurements and data analysis in Arizona are provided in Pandithurai et al. (1999).

Table 2. Monthly-mean spectral aerosol optical depths observed with the CIMEL Sky radiometer over Tombstone, Arizona during 1997. No measurements are available for April (λ is the wavelength).

λ (μm)	0.340	0.380	0.440	0.500	0.670	0.870	1.020
Month							
Jan	0.054	0.048	0.039	0.029	0.017	0.017	0.017
Feb	0.058	0.055	0.045	0.035	0.023	0.024	0.021
Mar	0.073	0.075	0.055	0.042	0.028	0.029	0.023
May	0.109	0.106	0.081	0.067	0.050	0.047	0.041
Jun	0.102	0.102	0.070	0.057	0.039	0.035	0.027
Jul	0.173	0.166	0.119	0.099	0.068	0.058	0.051
Aug	0.189	0.182	0.125	0.102	0.066	0.051	0.043
Sep	0.208	0.195	0.143	0.116	0.072	0.049	0.039
Oct	0.071	0.077	0.045	0.036	0.025	0.020	0.016
Nov	0.056	0.065	0.037	0.030	0.022	0.018	0.015
Dec	0.068	0.065	0.045	0.034	0.022	0.014	0.013

3. Numerical Experiments

3.1 Experiments Related to smoke

Possible ways of modeling the effect of aerosol (including smoke) on the surface irradiance were investigated in a series of numerical experiments. The experiments had different complexities; some considered only the effect of increased optical depth due to fires, while others took into account the change in optical properties in addition to the increase of particle concentration. Some of these experiments were performed on a global scale, while others were done only at locations where ground-measured irradiances were available. All experiments were carried

out for 1986 because of the availability of both satellite and ground data for that year. June was selected as the primary month for the study because biomass burning takes place in this month at locations where ground observations were available (primarily in a region bounded by 10S-5N and 15E-30E latitudes/longitudes). Some of the experiments were also performed for October 1986; however, results are not reported for this month because the high cloud cover masked the biomass burning effects. In all experiments, the D1 data from the International Satellite Cloud Climatology Project (ISCCP) were used.

In the numerical experiments, spatial and temporal distribution of the aerosol optical depth was described from three alternative sources:

1) Standard Radiation Atmospheres (SRA) (WCP-55, 1983)

2) GFDL GCTM

3) the Tegen et al. (1997) climatology

4) aerosol optical depth derived from ground-observed clear-sky transmittances.

The above optical depth climatologies were combined with aerosol optical properties from two models: 1) the Standard Radiation Atmospheres (SRA), and 2) the biomass burning (BMB) aerosol models described above. Various combinations of the optical depth climatologies and the optical properties were considered.

The following aerosol optical depth and aerosol optical properties combinations were used in the numerical experiments:

- Aerosol optical depth and optical property are from SRA (experiment without biomass burning correction (*SRA*))

- Aerosol optical depth was derived from observed clear-sky transmittances of DiPasquale et al. (1996). It was used to initialize the local aerosol climatology employed by the GEWEX/SRB algorithm. Only the amount of aerosol was changed in this experiment; the type and vertical distribution of aerosol used in the flux retrieval were specified according to the standard models SRA in WCP-55 (1983) (*Exp. 1*)

- The aerosol optical depth derived from clear-sky transmittances (see above) was combined with optical properties of Type-1 and Type-2 smoke from the model depicted in Figure 3 (*Exp. 2*)

- The aerosol optical depth derived from clear-sky transmittances (see above) was combined with optical properties of smoke from the biomass burning *BMB* model depicted in Figure 4 (*Exp. 3*)

- Aerosol optical depth is derived from the smoke map generated by the NOAA/GFDL GCTM (Stackhouse, Olson, Cahoon, private communication). The aerosol optical depth was calculated from the total particulate mass assuming a specific mass extinction cross-section of 9.6 m^2 g^{-1} at 550 nm (Anderson et al., 1996). The NOAA/GFDL GCTM smoke map gives only the optical depth associated with smoke. Therefore, the SRA climatology was used to supplement a "background: aerosol optical depth field. The optical properties are prescribed from the standard (*SRA*) aerosol models (*Exp. 4*)

- Aerosol optical depth is derived from the smoke map generated by the NOAA/GFDL GCTM. Total particulate matter was converted into initial optical depth values assuming a specific mass extinction cross-section of 4.6 m^2 g^{-1} at 550 nm [*Liousee et al.*, 1997]. Single scattering properties correspond to the smoke aerosol models (Types 1 and 2) described in section 2 (*Exp. 5*)

- Aerosol optical depth is derived from the smoke map generated by the NOAA/GFDL GCTM; optical properties are prescribed from the biomass burning (*BMB*) aerosol models (*Exp. 6*).

- Aerosol optical depth is from Tegen et al. (1997); optical properties are from SRA models (*Exp.* 7).

The GEWEX/SRB shortwave radiative-flux algorithm responds to increased values of aerosol loading if the increase is represented in the clear-sky radiance recorded in the satellite data. Since the effect of increased amount of aerosols on the clear-sky radiance might be similar to that caused by the presence of clouds, there is a potential for misidentification of pixels with bright smoke plumes as cloudy pixels. Such a misidentification leads to an overestimate of the cloud cover and an underestimate of the clear-sky reflectance. To explore the effect of this error on the derived surface shortwave flux, cloudy radiances were reassigned to clear-sky in a numerical experiment conducted for a single site. Only cloudy radiances that did not exceed the clear radiance by more than a certain threshold value were changed to clear radiances. The "revised" radiances then were used with different aerosol models in the GEWEX/SRB algorithm to retrieve surface fluxes in additional numerical experiments. The following combinations of radiances and aerosol models were used:

- "Revised" ISCCP-D1 radiance with SRA aerosol optical depth and optical property (*Exp. 8*);

- "Revised" ISCCP-D1 radiance with aerosol optical depth derived from the clear-sky transmittances of DiPasquale et al. (1996); optical properties are from the standard (SRA) aerosol model (*Exp. 9*);

- "Revised" ISCCP-D1 radiance with aerosol optical depth derived from the clear-sky transmittances of DiPasquale et al. (1996); optical properties are from the Type-2 smoke model of Liousse et al. (1997) and SRA models (*Exp. 10*);

- "Revised" ISCCP-D1 radiance with aerosol optical depth derived from the NOAA/GFDL chemical transport model; optical properties were from the biomass burning (BMB) models (*Exp. 11*).

3.2 Experiments Related to dust

The estimated surface SW radiative fluxes (global irradiance) used in this study are produced by NOAA/NESDIS, using the University of Maryland methodology (Pinker and Laszlo, 1992; Pinker et al., 1999). The algorithm is driven with observations made from the GOES-8 Imager, at hourly time intervals and at 0.5 degree spatial resolution over the domain of 25°-50° N, 67°-125° W. Each 0.5-degree grid cell is covered with 72 pixels of about 4 km resolution, which are used to determine whether it is clear or cloudy over the target. The satellite estimates of global irradiance have been previously evaluated on hourly, daily, and monthly time scales against observations made at about fifty stations during the year of 1996 (Pinker et al., 1999). For the interpretation of the satellite observations, use is made of the pre-launch calibration of GOES-8, as discussed in Weinreb et al., (1997). In the present study, validation over Arizona was expanded to include data from 1997, when aerosol optical depths were also observed.

We have performed an experiment to evaluate the sensitivity of surface SW radiative flux parameters to aerosol information. An off-line version of the SRB model was run for the entire year of 1997. All the satellite input parameters, as well as the atmospheric and surface parameters were the same as used by NOAA/NESDIS in the real time runs for 1997, and as archived at the University of Maryland. The only difference was that the climatological aerosol optical depth values used to initialize the retrieval process were replaced by the monthly mean observed values, as presented in Table 2. The impacts on the clear

sky fluxes (cloudless global irradiance), all sky fluxes (global irradiance), and surface albedo were explored.

4. Results

4.1 Results Related to smoke

Satellite-derived shortwave irradiances from all experiments and ground-observed daily and monthly downward surface shortwave irradiances (DiPasquale et al., 1996) were compared for June 1986. Experiments SRA and 7 were also carried out for the additional months of January, April and October of 1986. Figure 9 shows the result of the comparison for June 1986 from Experiment 6; statistics from Experiments 6 and 7 are also shown. In Figure10, the comparisons of observed and satellite-estimated irradiances are shown for the four months (January, April, June and October 1986). In this figure, the satellite-estimated fluxes were derived from using the SRA and Tegen et al. (1997) aerosol climatologies (Experiment 7). Bias and root-mean-square errors of monthly mean irradiances from selected Experiments for all 301 locations for June 1986 are summarized in Tables 2 and 3. Bias errors were calculated by subtracting the ground-measured irradiance from the satellite-estimated irradiance.

Table 3. Bias and RMS errors from selected Experiments

	Bias (satellite-ground) (Wm^{-2})	RMS (Wm^{-2})
SRA	2.7	27.3
Exp. 1	1.2	25.7
Exp. 5	1.1	27.6
Exp. 6	0.7	28.1
Exp. 7	4.5	27.1

Table 4. Bias and RMS errors (Wm-2) obtained from Experiments SRA and 7 for four months in 1986

	January	April	June	October
SRA	4.3/20.3	3.6/28.3	2.2/27.3	3.0/21.8
Exp. 7	6.7/20.6	5.6/28.2	4.5/27.1	5.5/21.6

When all stations are included, the bias and RMS errors from Experiments 1, 5, and 6 were 1-2 W m^{-2} and 26-28 W m^{-2},

respectively. These values represent only a modest change relative to those obtained with the standard SRA aerosol models. Large change in these values, however, is not expected since most of the 301 stations are not affected by biomass burning, and the uncertainties associated with each of the experiments and other input to the algorithm are similar. For this reason, a separate comparison was performed for 18 stations located in Africa (30S-12N; 5W-35E), which were known to experience smoke from biomass burning.

When the new aerosol models are used with the NOAA/GFDL-GCTM smoke map in the shortwave algorithm, the bias and root mean square errors in the monthly mean surface downward flux, for the 18 stations decrease by 5 W m^{-2} and 2 W m^{-2}, respectively. The results from selected Experiments for these locations are shown in Table 4.

Table 5. Bias and RMS errors for 18 stations in Africa.

	Bias (satellite-ground) (Wm^{-2})	RMS (Wm^{-2})
SRA	10.1	29.1
Exp. 5	-5.2	31.2
Exp. 6	-18.0	39.0

The initial aerosol optical depth values derived from the GCTM smoke plume range between 0.05 and 0.3 with a maximum at 7°S and 13°E (Figure 5, top panel). The map of final aerosol optical depth values obtained from the GEWEX/SRB algorithm (Figure 5, bottom panel) shows a range of 0.2-1.3, which is larger than the one from the GCTM smoke data. In addition, the area of increased optical depth is extended and the maximum is shifted to the northeast in comparison with the GCTM plume. The increase in aerosol optical depth is partly due to the fact that the final aerosol optical depth values are total values including both background aerosol and smoke, while those from the GCTM data are incremental values

The bias and root mean square errors are 2.7 W m^{-2} and 27.3 W m^{-2}, and 4.5 W m^{-2} and 27.1 W m^{-2} with the SRA (WCRP-55, 1983) and the Tegen et al. (1997) climatology, respectively. Although the bias error is almost doubled, the Tegen et al. aerosol climatology is preferred over the SRA. Its geographical and seasonal variation should be more realistic. It must be noted that in the current implementation of the Tegen et al. (1997) climatology, only the optical thickness values are used; the optical properties are still from the SRA aerosol models. This

might also contribute to the increased bias over certain areas.

To study the relative merits of the different biomass burning corrections on a regional scale, five African stations affected by smoke, as determined from the GCTM smoke map, were selected. The latitude-longitude coordinates of these stations are as follows:

Site	Lat	Lon
Buta	2.783 N	24.783 E
Inongo	1.967 S	18.267 E
Kananga	5.883 S	22.417 E
Kinshasa	4.367 S	15.250 E
Mbandaka	0.050 N	18.267 E

Two stations (Kinshasa and Kananga) were directly located in an area where burning usually takes place [*Konzelmann et al.*, 1996]. The other three stations (Buta, Mbandaka and Inongo) are likely to be affected by smoke transported over by the wind in June. Daily average shortwave downward fluxes calculated from the numerical experiments were compared with observed fluxes. The latter were available from the GEBA archive (Ohmura and Gilgen, 1991). The biomass burning correction applied in the different experiments reduced the bias errors in most cases; the root-mean-square (RMS) errors, however, did not change significantly. This suggests that most of the reduction in the bias is a result of cancellations of errors in the daily estimates. No single experiment can be selected to work the best for all five stations. In most cases, however, the application of the smoke aerosol model, and a better initialization of the aerosol optical depth resulted in decreased biases. Examples of the bias and RMS differences obtained from Experiments SRA, 6, 7 and 8 are shown in Figure 11.

For Kananga and Mbandaka, the smallest errors were obtained from Experiment 8, when the optical thickness values derived from the clear-sky transmittances were used to initialize the aerosol optical thickness in the algorithm, and some of the cloudy radiances were reassigned to clear radiances (thus the cloud cover were also changed). For example, for Kananga, Africa the bias in the daily downwelling shortwave flux in June 1986 was reduced 9.2 W m^{-2} to 1.5 W m^{-2} and the RMS error was reduced 5.8 W m^{-2} to 32.3 W m^{-2}. In the top panel of Figure 12, the absolute values of the difference between the clear and cloudy scaled radiances as reported in the ISCCP data are plotted at a particular hour for the days in June for this location. As can be seen, for the second part of the month this difference is very small. In Experiment 8, cloudy radiances that were smaller than 0.05 were associated with "bright smoke" and reclassified as clear radiances. In the bottom panel of Figure 12, the time series of the daily average shortwave irradiances obtained

from Experiment 8 and from observation is displayed. For comparison, daily irradiances derived from the SRA aerosol climatology are also plotted. As evident, there is a significant improvement in the agreement between the observed irradiance and the one obtained from Experiment 8 on days for which the cloudy radiances were changed to clear radiances.

4.3 Results Related to dust

4.3.1 Surface downwelling shortwave fluxes

In Figure 13a, a comparison between instantaneous clear-sky radiative fluxes as derived from GOES-8 observations over a satellite grid closest to Tucson is presented for the month of June 1997. One set of inferred values was obtained from the routine run (control run), using aerosol climatology (optical depth, τ_c), while the other set was obtained with off-line run, using monthly mean observed values of aerosol optical depth (τ_o). The mean of the instantaneous fluxes from the "control" run was 789.0 Wm^{-2}, while the observed aerosol climatology yielded a 14.0 Wm^{-2} higher value (803.0 Wm^{-2}). Since the assumed average aerosol optical depth climatology for June was 0.230, while the measured value was 0.057, the effect should indeed be to increase the downward fluxes at the surface. June 1997 was a predominantly clear month, therefore, the results for the all-sky cases (Figure 13b) are similar. The mean instantaneous fluxes from the control run and from the experimental run were 750.1 Wm^{-2} and 763.5 Wm^{-2}, respectively. Using the Student's t test on paired data, for both clear and cloudy skies, has shown that the above means are significantly different at the 0.05 level.

A comparison of hourly mean estimated global irradiance with ground truth as obtained from the control run, is presented in Figures 14 for all sky (a) and clear sky (b) cases independently. In Figure 15, the comparison was repeated using results from the experimental run. For clear sky there is a clustering of data because the solar zenith angle is changing only by a small amount at a particular instant from one day to another (the same clustering is observed in Figure 13a). For all-sky conditions, the gaps between the clear-sky clusters are filled with values observed for different levels of cloudiness. The correlation between satellite derived fluxes and those measured at the ground is very high for both cloudy and cloudless conditions (0.96-0.99) which is due to the dominance of the external solar forcing from one hour to another. The largest scatter occurs in the gaps between the clear-sky clusters, pointing to existing uncertainties in the retrieval of global irradiance for cloudy conditions. The use of observed values of aerosol optical depth reduced

the bias for both all sky and clear sky cases by about 12-13 Wm^{-2}, and improves the rms by about 4-7 Wm^{-2}. The smaller rms errors suggest that the reduction in bias is not purely because of better cancellation of errors. Just as it has been found for the satellite-estimated instantaneous global irradiance, Student's t test on paired data showed that the hourly mean fluxes estimated from the two initializations are significantly different at the 0.05 level. The probability of obtaining a t value larger than that obtained (-15.4 for all sky, -14.7 for clear sky) by chance alone when the two means are not different is negligible ($3*10^{-40}$ for all sky, $4*10^{-39}$ for clear sky).

It was found that the current satellite estimates are within 70 Wm^{-2} of the ground observations on an hourly time scale, and within 24 Wm^{-2} on a daily time scale. In the latter case, this is less than 10% of the mean. Use of actual observations of aerosols, as compared to climatological values, reduces the bias substantially, while less significant changes in the rms were found.

4.3.2 Surface albedo

The GCIP/SRB model produces surface downwelling and upwelling SW radiative fluxes (global and reflected radiation), and their ratio is termed "albedo". At instantaneous time scales, the albedo represents the value at the time of the observation. In order to derive a daily value, the downwelling and upwelling fluxes are averaged and their ratio is taken. Since the surface fluxes are computed independently for clear and cloudy pixels, it is possible to produce "clear sky" albedos and all-sky albedos. Preliminary evaluations show that these two values are quite close to each other. In Figure 16, ten predominantly clear days in June were selected to study the diurnal variation of the surface albedo over Tucson, AZ, and to evaluate the effect of aerosol initialization. In the left panel, climatological aerosol values were used; in the middle panel, the observed values were used; and the right panel represents the difference. As evident, the albedos are somewhat higher when aerosol observations are used. This is consistent with the fact that the observed aerosol optical depth was found to be lower than the assumed climatological value. Therefore, the decreased aerosol contribution to the satellite observed top of the atmosphere albedo had to be compensated by an increase of surface albedo.

Software developed under the project

- IDL and Fortran programs, C-shell scipts to read and remap the GFDL/GCTM smoke maps and the Tegen et al. monthly aerosol data,

- Fortran programs to interface the global aerosol data with the GEWEX/SRB algorithm,
- Fortran program to invert the clear-sky transmittance data of DiPasquale et al

Presentations resulting from project

Holben, B. N., D. Tanre, A. Smirnov, T. F. Eck, I. Slutsker, N. Abuhassen, W. W. Newcomb, J. Schafer, B Chatenet, F. Lavenue, Y. J. Kaufman, J. Vande Castle, A. Setzer, B. Markham, D. Clark, R. Frouin, R. Halthore, A. Karnieli, N. T. O'Neill, C. Pietras, R. T. Pinker, K. Voss, G. Zibordi, 2000. An emerging ground-based aerosol climatology: Aerosol Optical Depth from AERONET. Submitted for publication in Journal of Geophysical Research.

Laszlo, I., and R. T. Pinker, 1999: Modeling direct radiative effects of aerosols in the GEWEX/SRB shortwave algorithm*AMS 10th Conference on Atmospheric Radiation*, Madison, Wisconsin, 28 June-2 July 1999.

Laszlo, I., and R. T. Pinker, 1999: An improved treatment of aerosol radiative effects in the GEWEX/SRB shortwave algorithm, *The Third International Scientific Conference on Global Energy and Water Cycle,* Beijing, China, 16-19 June 1999.

Laszlo, I., 1998: Correcting for biomass burning in the GEWEX/SRB shortwave algorithm, Solar Radiation and Climate, Gordon Research Conferences, Plymouth, New Hampshire, June 14-19, 1998.

Pandithurai, G., R. T. Pinker, O. Dubovik, B. N. Holben, and T. O. Aro, 2000. Dust Aerosol Climatology in the sub-Sahel. Submitted for publication in JGR.

Pinker, R. T., P. Govindand, B. N. Holben, O. Dubovik, and T. O. Aro, 2000. On the importance of real-time observations of dust aerosol properties. For publication in JGR.

Pinker, R. T., I. Laszlo, D. Goodrich, and G. Pandithurai, 2000. Satellite Estimates of Surface Radiative Fluxes for the Extended San Pedro Basin: Sensitivity to Aerosols.Agric. And Forest Meteorology, in press.

References

Ackerman S. A. and S. K. Cox, 1982. The Saudi Arabian heat low: Aerosol distributions and thermodynamic structure. J. Geophys. Res., 87, 8991-9002.

Anderson, B. E., W. B. Grant, G. L. Gregory, E. V. Browell, J. E. Collins Jr., G. W. Sachse, D. R. Bagwell, C. H. Hudgins, D. R. Blake, and N. J. Blake, 1996. Aerosols from biomass burning over the tropical South Atlantic region: Distributions and impacts, *J. Geophys. Res.*, **101**, 24117-24137.

Archive (GEBA). World Climate Program-Water Project A7, Rep. 2: The GEBA Database, Verlag der Fachvereine, 60 pp.

Cahoon, D. R., Jr., B. J. Stocks, J. S. Levine, W. R. Cofer III, and K. P. o'Neill, 1992. Nature, 359, 812-815.

Charlson, R, J. et al., 1987. Nature, 326, 655.

Charlson, R. J. et al., 1991. Tellus, Ser. AB 43, 152.

d'Almeida, G. A. and L. Schutz, 1983. Number, mass and volume distribution of mineral aerosol and soils in the Sahara. J. Clim. Appl. Meteor., 22, 233-243.

d'Almeida, G. A., P. Koepke, and E. P. Shettle, 1991. Atmospheric aerosols: Global climatology and radiative characteristics. A. Deepak Publishing, Hampton, VA, pp. 561.

d'Almeida, G. A., 1986. A model for Saharan dust transport. J. Clim. Appl. Meteor., 25, 903-916.

DiPasquale, R. C., Quigley, P. A., Whitlock, C. H., Tsvetkov, A., and Wilcox, S., 1986. Daily Daylight Cloud Fraction, Shortwave Surface Radiation, and Transmittance for 502 Sites. NASA Tech. Mem. TM-110245, 359 pp., 1996.

Ferrare, R. A., R. S. Fraser, and Y. J. Kaufman, 1990. J. Geoph. Res., 95, 9911.

Houghton, R. A., 1944. Bioscience, 44, 305-313.

Keeling, C. D., T. P. Whorf, M. Wahlen, and J. van der Plicht, 1995. Interannual extremes in the rate of rise of atmospheric carbon dioxide since 1980. Nature, 375,666-670.

Konzelmann, T., D. R. Cahoon, and C. H. Whitlock, 1996. Impact of biomass burning in equatorial Africa on the downward surface shortwave irradiance: Observations versus calculations, *J. Geophys. Res.*, **101**, 22833-22844.

Liousse, C., F. Dulac, H. Cachier, and D. Tanré, Remote sensing of carbonaceous aerosol production by African savanna biomass burning, 1997. *J. Geophys. Res.*, **102**, 5895-5911.

Pandithurai, G., R. T. Pinker, and B. Holben, 1999. Annual variation of aeroslo optical properties in a semi-arid region as observed within the Aeronet framework. 10th *Conference on Atmospheric Radiation, Madison, Wisconsin, 26 June-2 July, 1999.*

Patterson, E. M. and D. A. gillette, 1977. Commonalities in measured size distributions for aerosols having a soil-derived component. J. Geophys. Res., 82, 2074-2082.

Penner, J. E., R. E. Dickinson, C. A. O'Neill, 1992. Effects of aerosols from biomass burning on the global radiation budget. Science, 256, 1432-1434.

Pinker, R. T. and I. Laszlo, 1992. Modeling surface solar irradiance for satellite applications on a global scale. J. Appl. Meteor., 31, 194-211.

Pinker R. T. J. D. Tarpley, I. Laszlo, and K. Mitchell, 1999. Surface radiation budgets in support of the GEWEX Continental Scale International Project (GCIP). Submitted for publicatiuon in *J. Geophys. Res.*

Radke, L. F. et al., 1988. Aerosols and climate. P. V. Hobbs and M. P. McCormick, Eds. (Deepak, Hampton, VA, pp. 411-422.

Rosen, H. and T. Novakov, 1984. Role of graphitic carbon particles in atmospheric radiation on transfer, in: Aerosols and their climatic effects (H. E. Gerber and A. Deepak, eds.), A. Deepak Publishing, Hampton, VA, 83-94.

Rossow, W. B., and R. A. Schiffer, 1991. ISCCP cloud data products. Bull. Amer. Meteor. Soc., 72, 2-20.

Schiffer, R. A. and W. B. Rossow, 1985. ISCCP global radiance data set: A new resource for climate research. Bull. Amer. Meteor. Soc., 66, 1498-1505.

Schutz, L. and R. Jaenicke, 1974. Particle number and mass distribution above 10-4 cm radius in sand and aerosol of the Sahara desert. J. Appl. Meteor., 13, 863-870.

Seiler, W., and P. J. Crutzen, 1980. Climate Change, 2, 207.

Tegen, I., P. Hollrig, M. Chin, I. Fung, D. Jacob, and J. Penner, 1997. Contribution of different aerosol species to the global aerosol extinction optical thickness: Estimates from model results. *J. Geophys. Res.*, **102**, 23895-23915.

Twitty, J. T. and J. A. Weinman, 1971. Radiative properties of carbonaceous aerosols. J. Appl. Meteor., 10, 725-731.

Twomey, S., 1971. J. Atmos. Sci., 28, 1149.

Weinreb, M. P., M. Jamieson, N. Fulton, Y. Chen, J. X. Johnson, J. Bremer, C. Smith, and J. Baucom, 1997. Operational calibration of Geostationary Operational Environmental Satellite-8 and -9 imagers and sounders. *Applied Optics*, **36**, *6895-6904, 1997*.

Whitlock, C. H., D. Cahoon, and T. Konzelman, 1995. Biomass burning effects on satellite estimates of shortwave surface radiation in Africa. Submitted for publication in Biomass Burning and Global Change.

WCP-55, 1983. Aerosols and their Climatic Effects, edited by A. Deepak and H. E. Gerber, 107 pp., WMO, Geneva, 1983.

List of Figures:

Figure 1 Size distribution functions of Type-1 and Type-2 aerosol models. OC-organic carbon; BC-black carbon; WS-water soluble, N-number density; r-radius. The numbers in parentheses are the volume mean radii in micrometers.

Figure 2 Coefficients of absorption and extinction, single-scattering albedo and asymmetry parameter for the Type-2 model components of organic carbon (OC), black carbon (BC), dust-like (Dust), and water soluble particles (WS) (top four panels), and for the smoke models of Type-1, Type-2 and continental (CONT-I) aerosol (bottom four panels). The particle number concentrations used are such that the extinction coefficients are 1 km^{-1} at the wavelength of 0.55 μm.

Figure 3 Vertical profiles of aerosol adopted for use over land, water and for biomass smoke (Cont-I, Mar-I, Smoke-1 and Type-2 aerosol models. Listed for each layer are the extinction coefficient (black), single-scattering albedo (red), asymmetry parameter (green), and extinction optical depth (violet). All values refer to the wavelength of 0.55 μm. All parameters are constant within the layers, except for the extinction coefficient above 20 km where it varies linearly with altitude.

Figure 4 Aerosol models adopted for large-scale (250x250 km) scenes. Biomass burning (BMB) profiles are obtained by weighting the profiles shown in Figure 3 (see Figure 3 for explanation)

Figure 5 Distribution of aerosol optical thickness (0.55 •m) derived from the GFDL Chemical Transport Model (CTM) for June 1986 for Africa (top), and that obtained from the GEWEX/SRB shortwave algorithm (bottom). The GFDL/CTM optical depth field was used to initialize the aerosol optical depth in the algorithm. Three-hourly values of the aerosol optical depth then were obtained from the ISCCP-D1 clear-sky radiances.

Figure 6 Aerosol optical depth climatology built from the Standard Radiation Atmospheres (SRA) (top). Difference of aerosol optical depth fields for June obtained by subtracting the SRA climatology from the Tegen et al. climatology (bottom).

Figure 7 Aerosol optical depth derived from clear-sky transmittances of DiPasquale et al. (1996) for June 1986.

Figure 8 Frequency of methods used to determine the monthly clear-sky transmittances of DiPasquale et al. (1996).

Figure 9 Comparison of observed flux with that estimated from satellite in *Experiment 6* for June 1986. Closed circles are for 18 stations in Africa. Bias (satellite-ground) and root mean square errors (Wm^{-2}) are shown for *Experiment 6* and 7.

Figure 10 Comparison of observed monthly mean shortwave irradiance with irradiance estimated from satellite data using the standard SRA aerosol climatology (top) and the Tegen et al. (1997) climatology (bottom). Irradiances were derived for January, April, June and October 1986. Bias (satellite-ground) and root mean square (RMSE) differences in Wm^{-2} are also shown.

Figure 11. Bias (satellite-ground) and root mean square (RMS) differences (Wm^{-2}) of daily shortwave surface irradiances for five stations affected by biomass burning in Africa in June 1986. Irradiances were estimated from ISCCP D1 satellite data using the standard SRA aerosol climatology, and in *Experiments 6, 7* and *8*.

Figure 12 Difference of cloudy and clear scaled radiances in the ISCCP D1 data for a single cell (2876) in June 1986 (top). Comparison of observed and satellite-estimated daily surface irradiance for ISCCP cell 2876 for June 1986 (bottom panel). The satellite-estimated irradiances were obtained in *Experiment 8*.

Figure 13. Comparison of instantaneous clear-sky (a) and all-sky (b) surface global irradiances, ($W\ m^{-2}$) retrieved using the two different initializations of the aerosol optical depth (observed, τ_o and climatological, τ_c). The global irradiances were obtained from the NOAA/NESDIS GCIP product for June 1997 for the 0.5-degree grid box containing Tucson, AZ.

Figure 14. Comparison of hourly mean all-sky (a) and clear-sky (b) surface global irradiance derived from the NOAA/NESDIS GCIP product with ground observations, for June 1997, Tucson, AZ. Aerosol optical depth was initialized with climatological values in the retrieval (the diagonal is the line of perfect agreement; **rms**: root mean square error in $W\ m^{-2}$;

bias: satellite-estimated flux minus measured flux in W m^{-2}; **r**: correlation coefficient).

Figure 15. The same as Figure 6, but observed values of aerosol optical depth were used for initialization in the retrieval of the surface global irradiance.

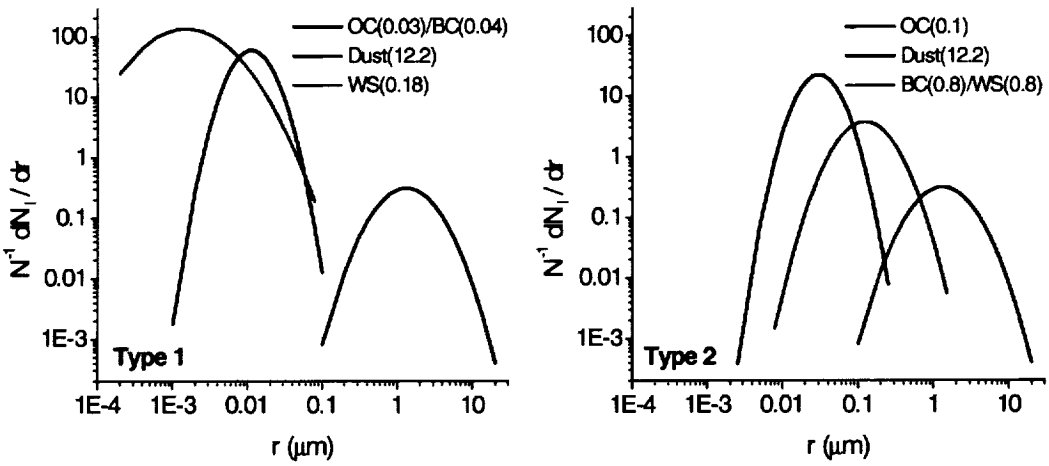

Figure 1. The size distribution functions of Type-1 and Type-2 aerosol models. OC-organic carbon; BC-black carbon; WS-water soluble; N-number density; r-radius. The numbers in parentheses are the volume mean radii in micrometers.

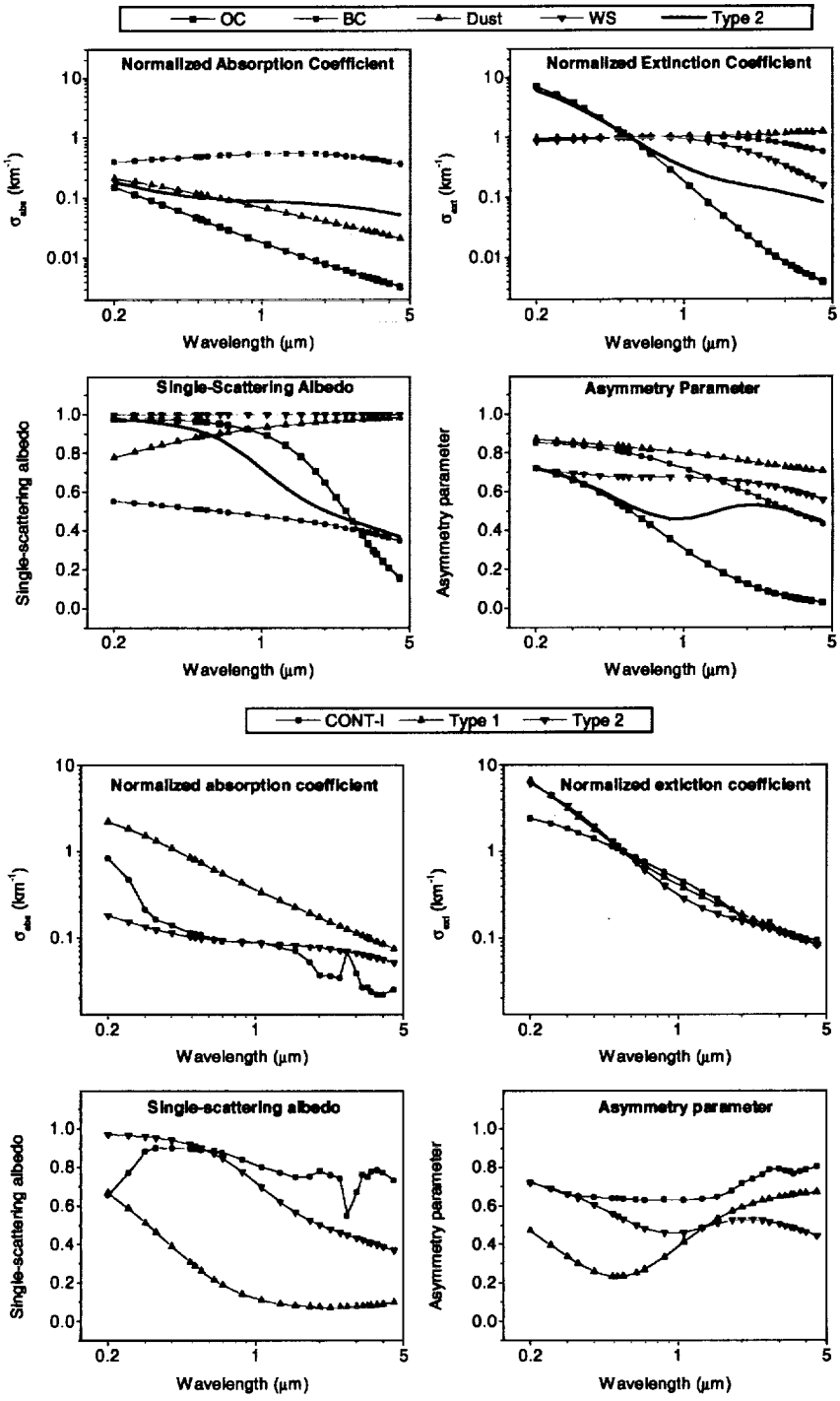

Figure 2. Coefficients of absorption and extinction, single-scattering albedo and asymmetry parameter for the Type-2 model components of organic carbon (OC), black carbon (BC), dust-like (Dust), and water soluble particles (WS) (top four panels), and for the smoke models of Type-1, Type-2 and continental (CONT-I) aerosol (bottom four panels). The particle number concentrations used are such that the extinction coefficients are 1 km^{-1} at the wavelength of 0.55 μm.

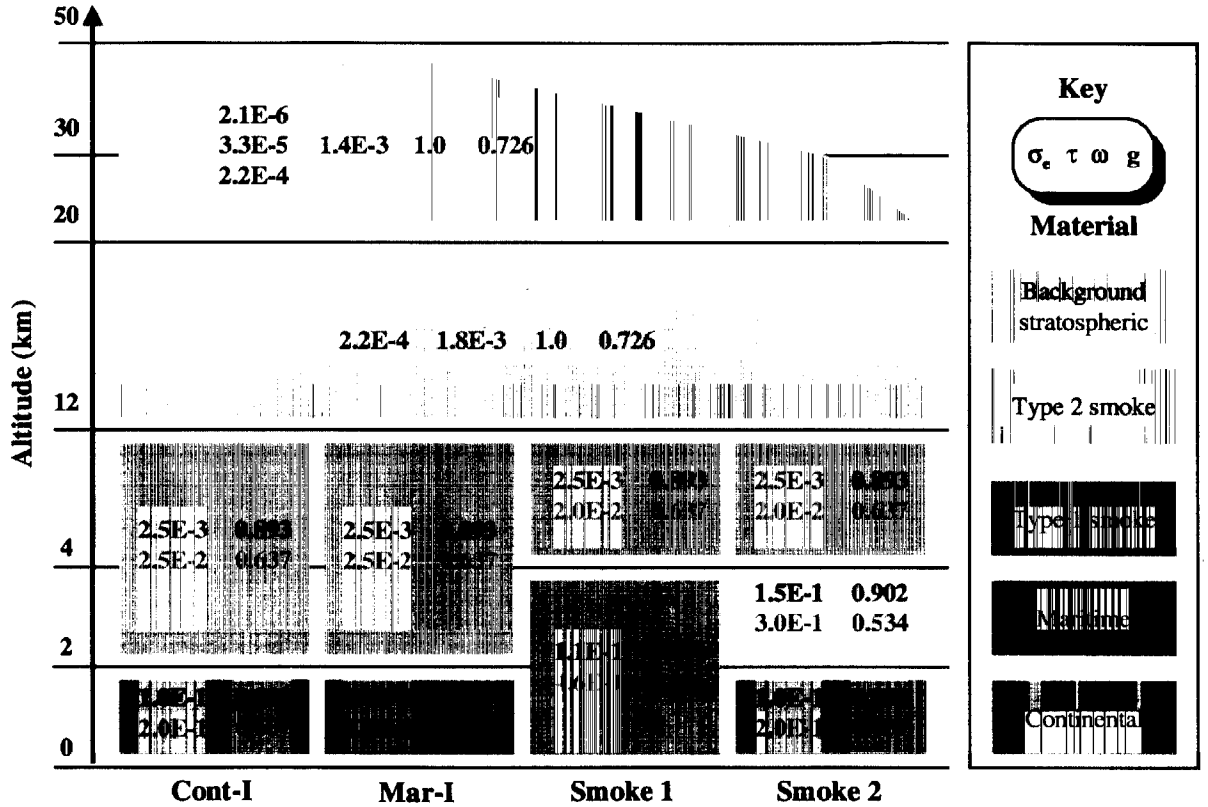

Figure 3. Vertical profiles of aerosol adopted for use over land, water and for biomass smoke (Cont-I, Mar-I, Smoke-1 and Type-2 aerosol models. Listed for each layer are the extinction coefficient (black), single-scattering albedo (red), asymmetry parameter (green), and extinction optical depth (violet). All values refer to the wavelength of 0.55 μm. All parameters are constant within the layers, except for the extinction coefficient above 20 km where it varies linearly with altitude.

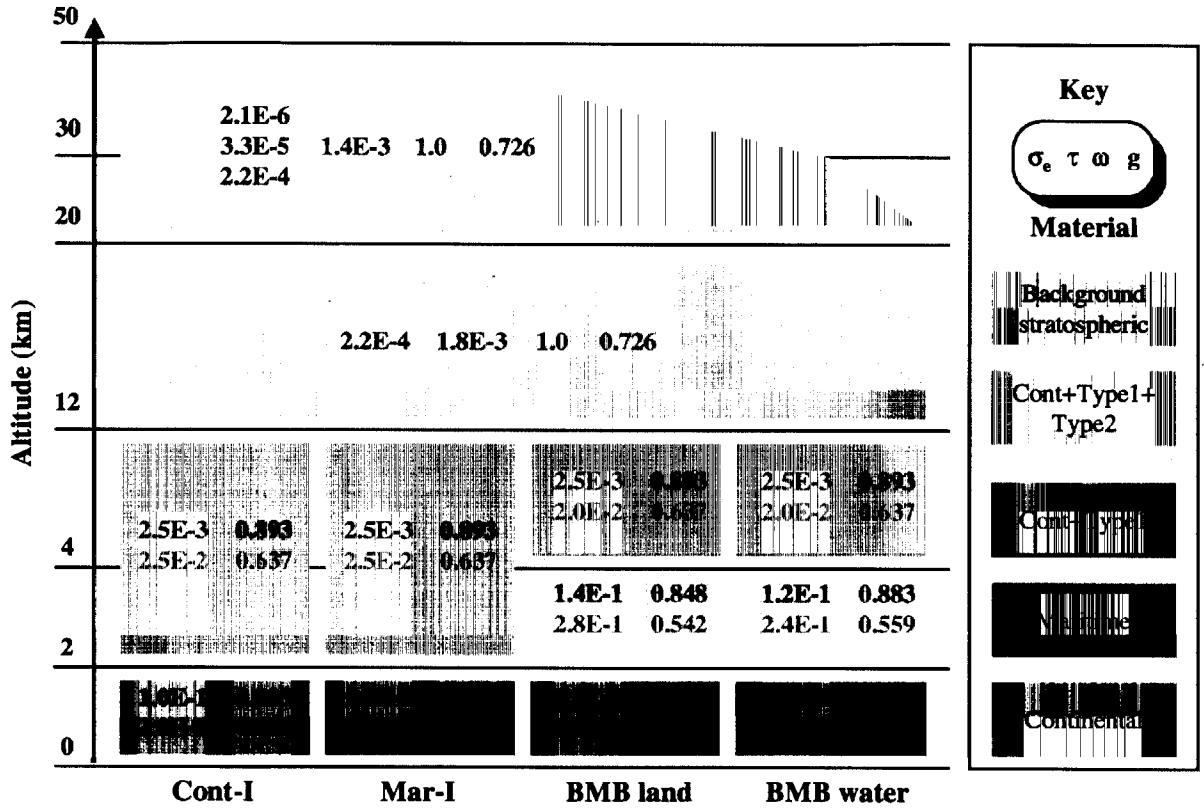

Figure 4. Aerosol models adopted for large-scale (250x250 km) scenes. Biomass burning (BMB) profiles are obtained by weighting the profiles shown in Figure 3. (See Figure 3 for explanation.)

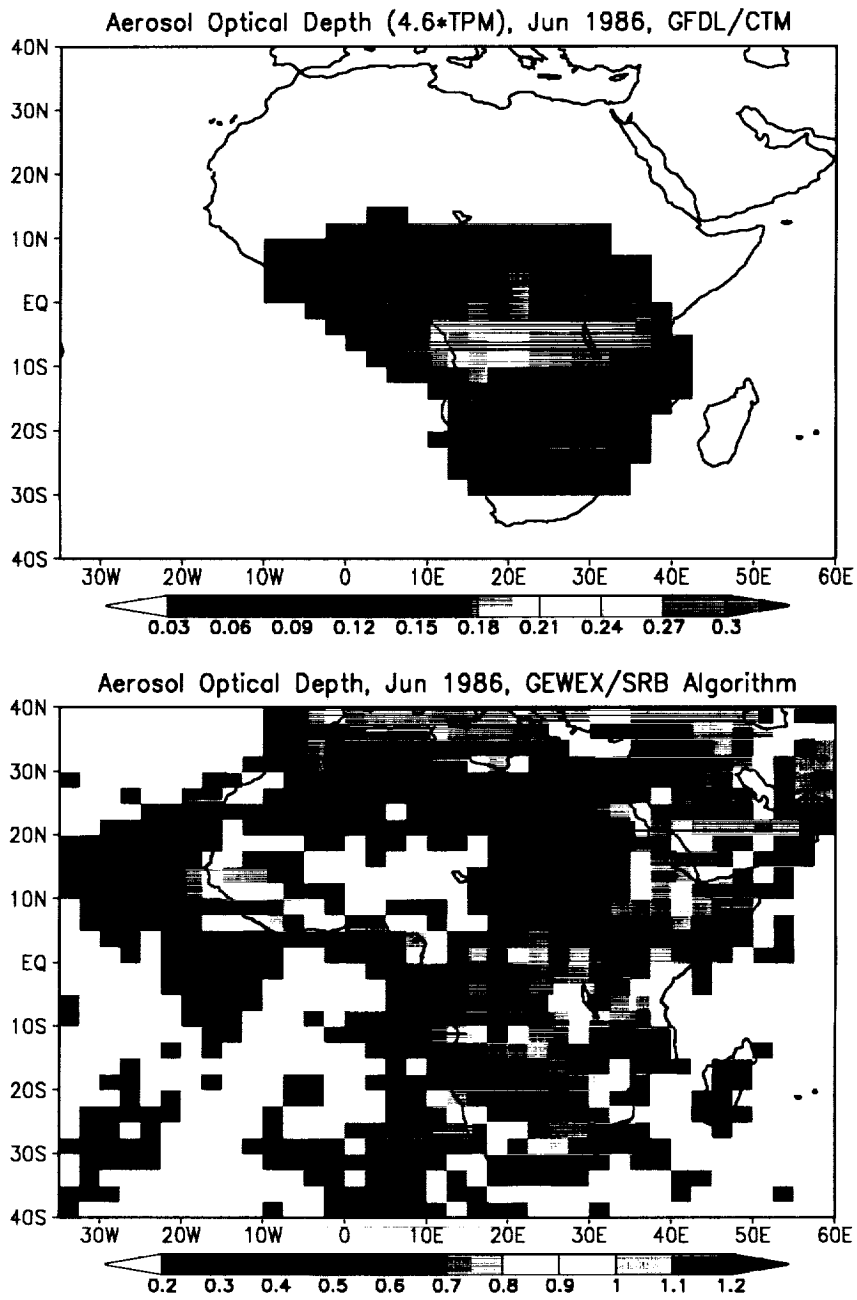

Figure 5. Distribution of aerosol optical thickness (0.55 μm) derived from the GFDL Chemical Transport Model (CTM) for June 1986 for Africa (top), and that obtained from the GEWEX/SRB shortwave algorithm (bottom). The GFDL/CTM optical depth field was used to initialize the aerosol optical depth in the algorithm. Three-hourly values of the aerosol optical depth then were obtained from the ISCCP-D1 clear-sky radiances.

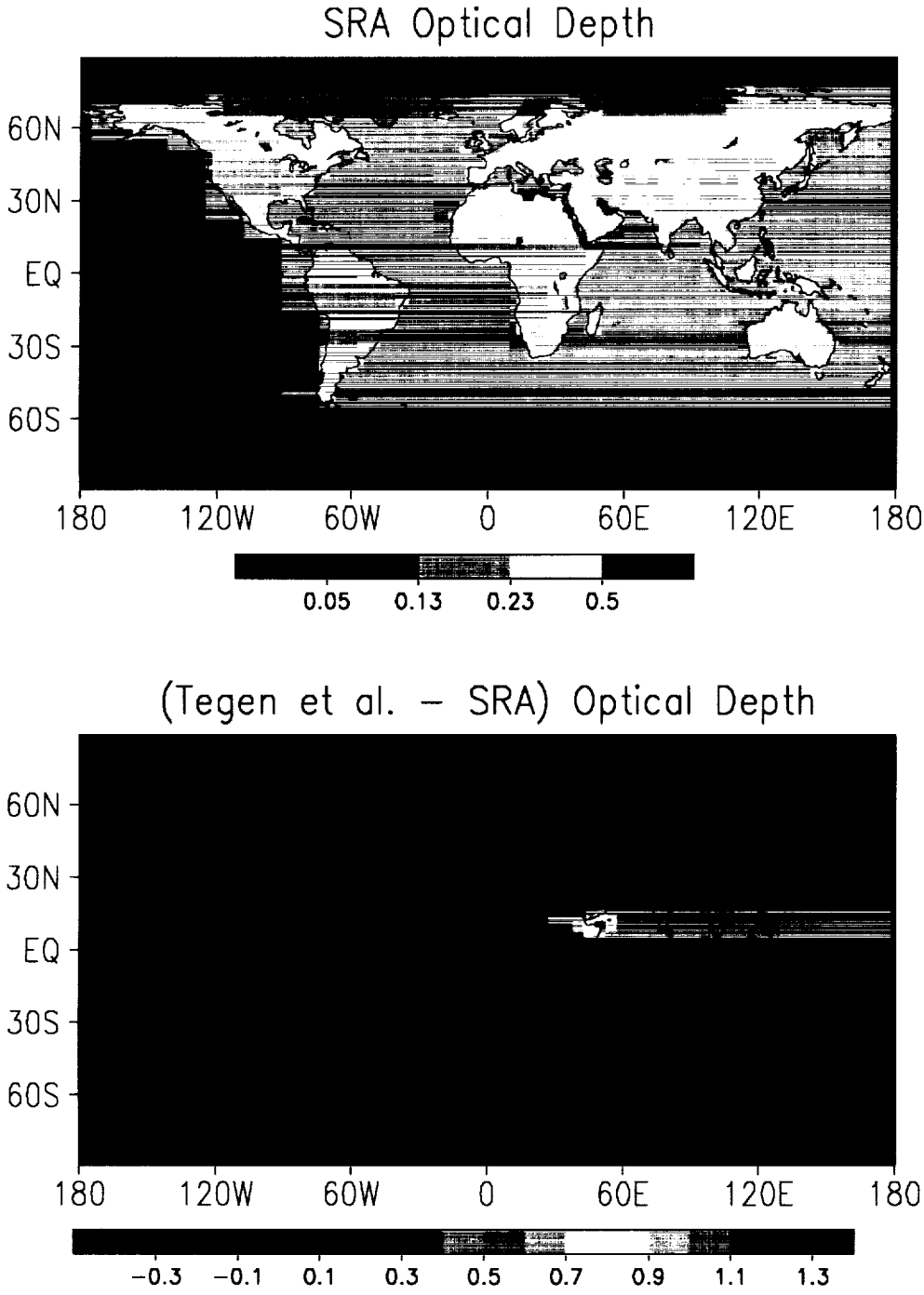

Figure 6. Aerosol optical depth climatology built from the Standard Radiation Atmospheres (SRA) (top). Difference of aerosol optical depth fields for June obtained by subtracting the SRA climatology from the Tegen et al. climatology (bottom).

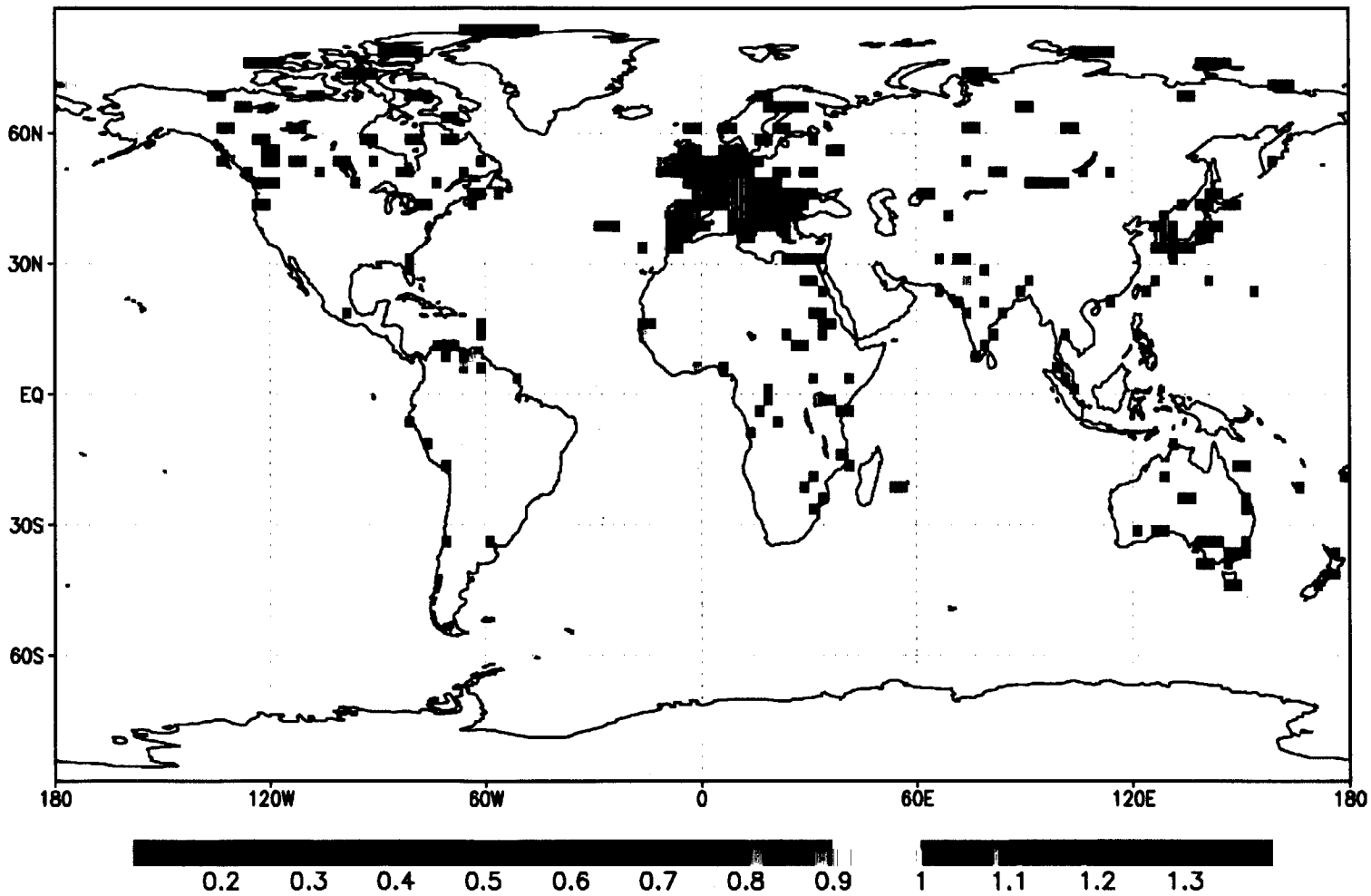

Figure 7. Aerosol optical depth derived from clear-sky transmittances of DiPasquale et al. (1996) for June 1986.

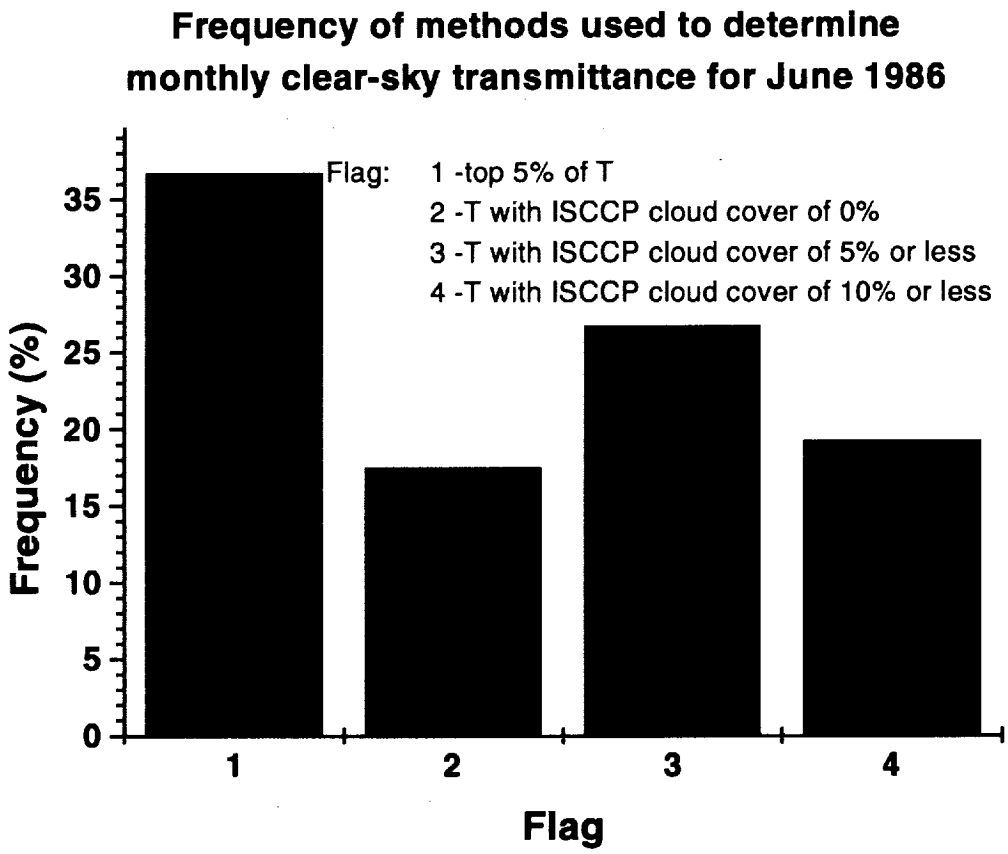

Figure 8. Frequency of methods used to determine the monthly clear-sky transmittances of DiPasquale et al. (1996).

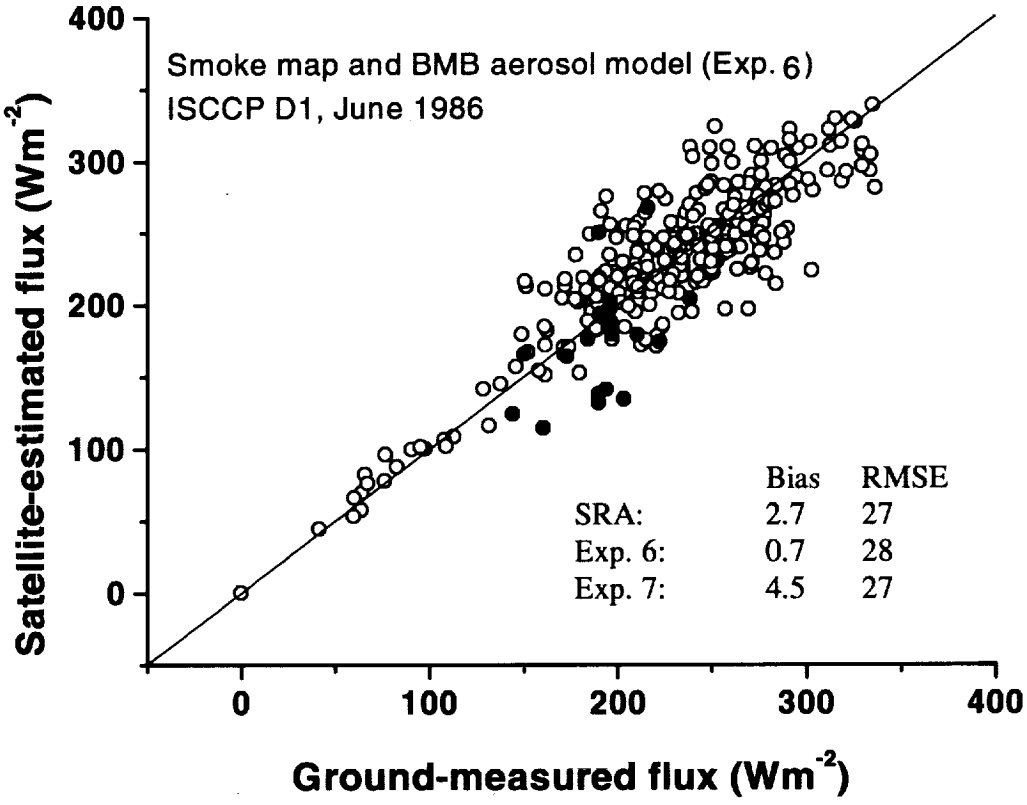

Figure 9. Comparison of observed flux with that estimated from satellite in *Experiment 6* for June 1986. Closed circles are for 18 stations in Africa. Bias (satellite-ground) and root mean square errors (Wm^{-2}) are shown for *Experiment 6* and 7.

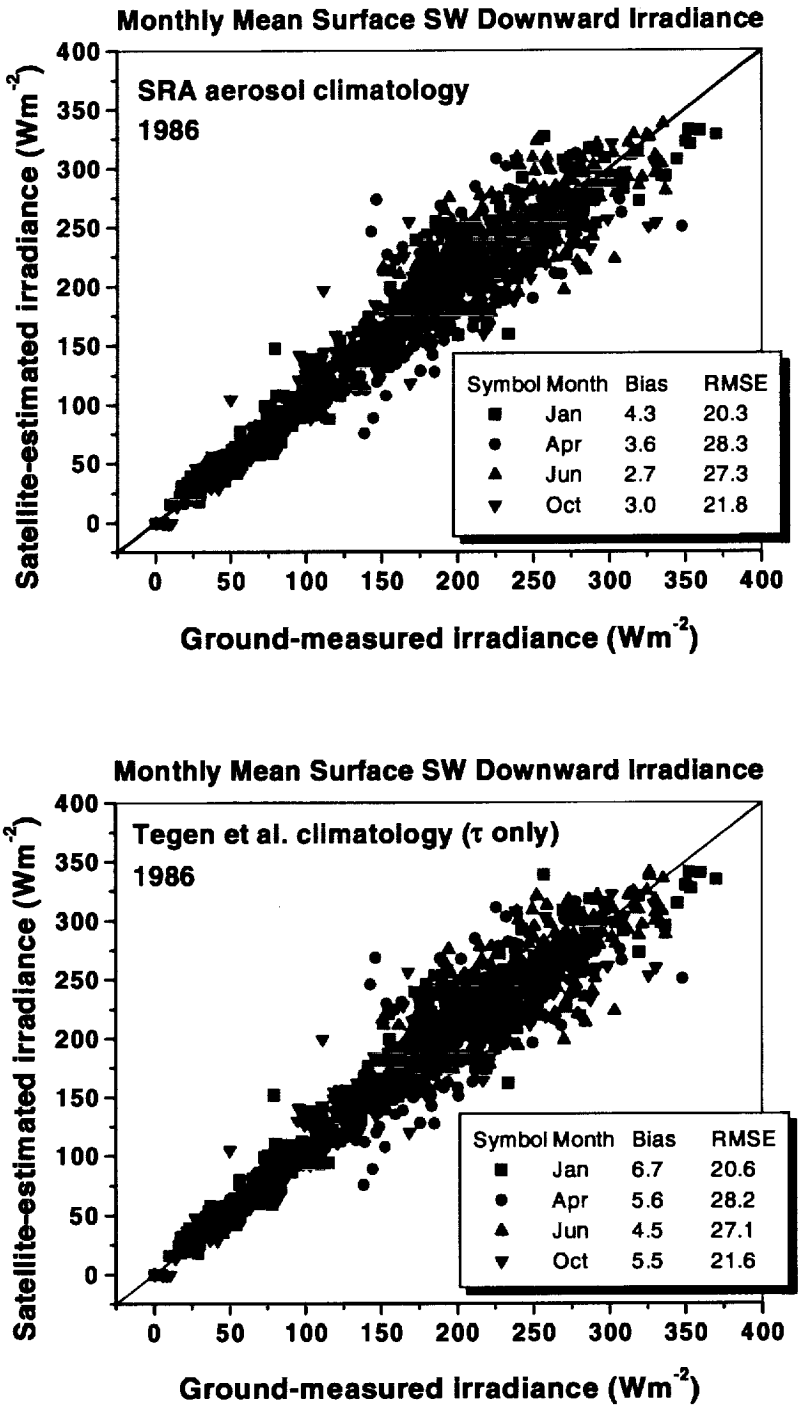

Figure 10. Compariosn of observed monthly mean shortwave irradiance with irradiance estimated from satellite data using the standard SRA aerosol climatology (top) and the Tegen et al. (1997) climatology (bottom). Irradiances were derived for January, April, June and October 1986. Bias (satellite-ground) and root mean square (RMSE) differences in Wm^{-2} are also shown.

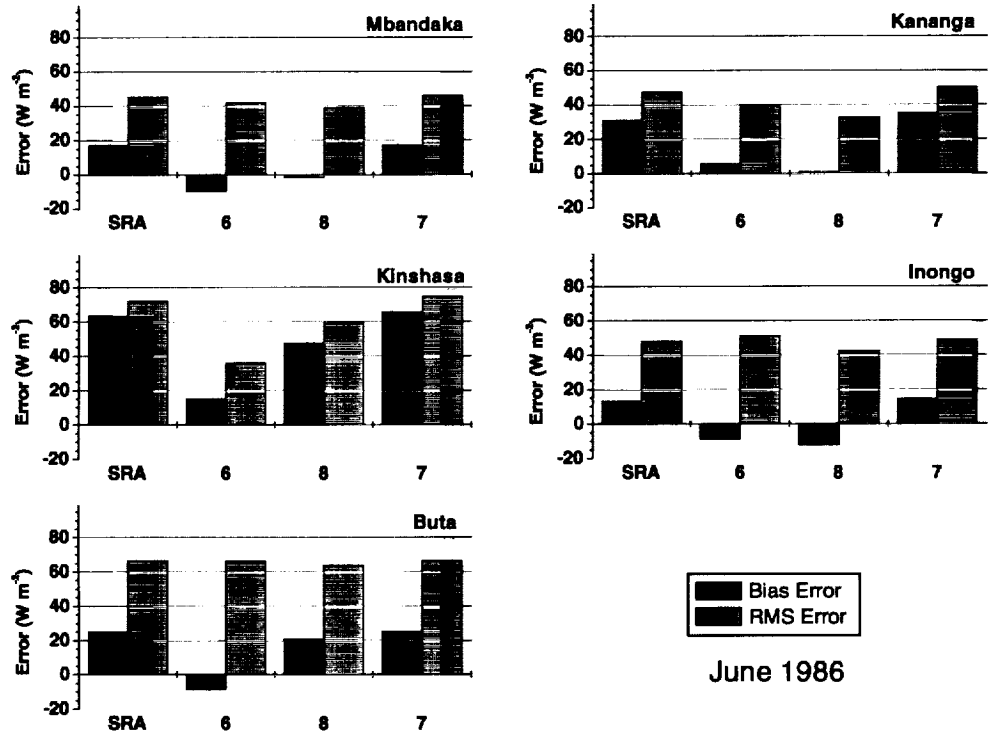

Figure 11. Bias (satellite-ground) and root mean square (RMS) differences (Wm^{-2}) of daily shortwave surface irradiances for five stations affected by biomass burning in Africa in June 1986. Irradiances were estimated from ISCCP D1 satellite data using the standard SRA aerosol climatology, and in *Experiments 6, 7* and *8*.

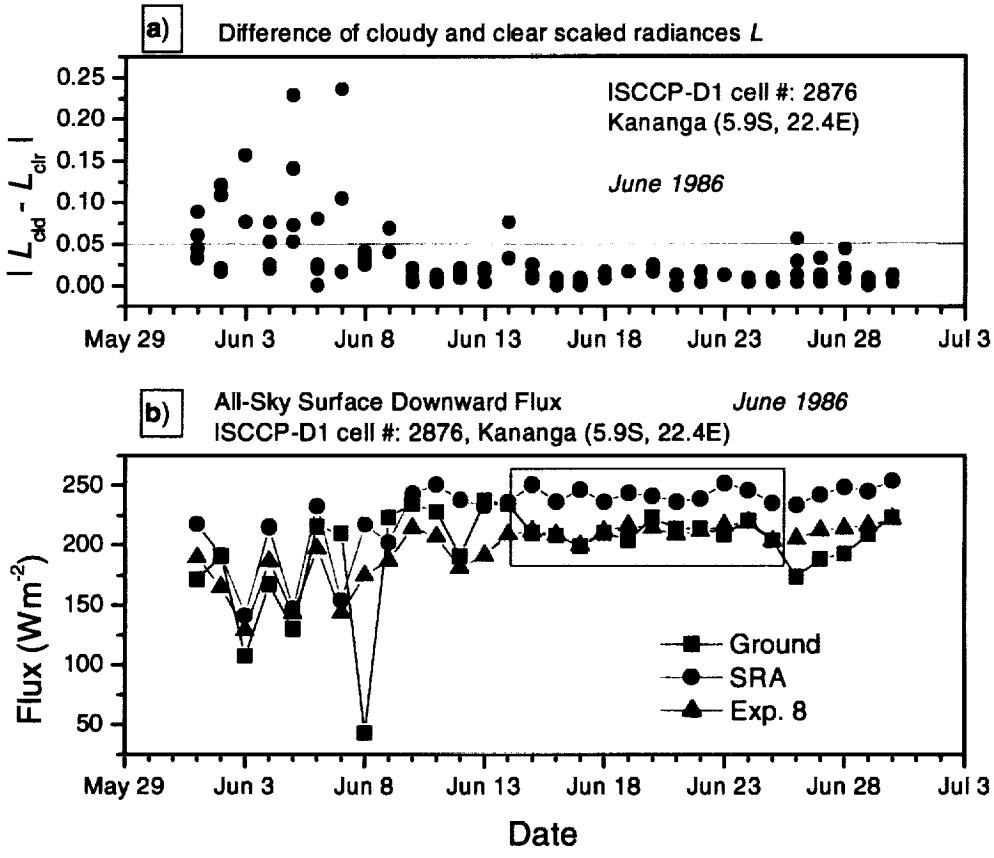

Figure 12. Difference of cloudy and clear scaled radiances in the ISCCP D1 data for a single cell (2876) in June 1986 (top). Comparison of observed and satellite-estimated daily surface irradiance for ISCCP cell 2876 for June 1986 (bottom panel). The satellite-estimated irradiances were obtained in *Experiment 8*.

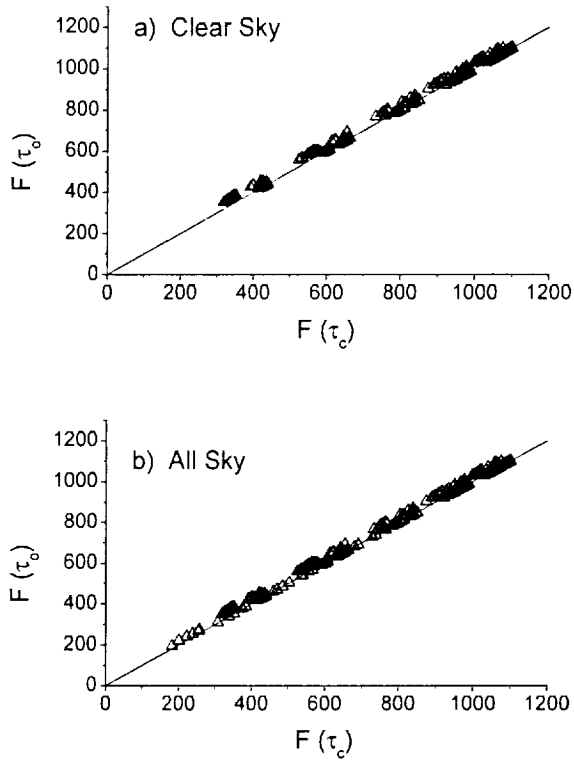

Figure 13.

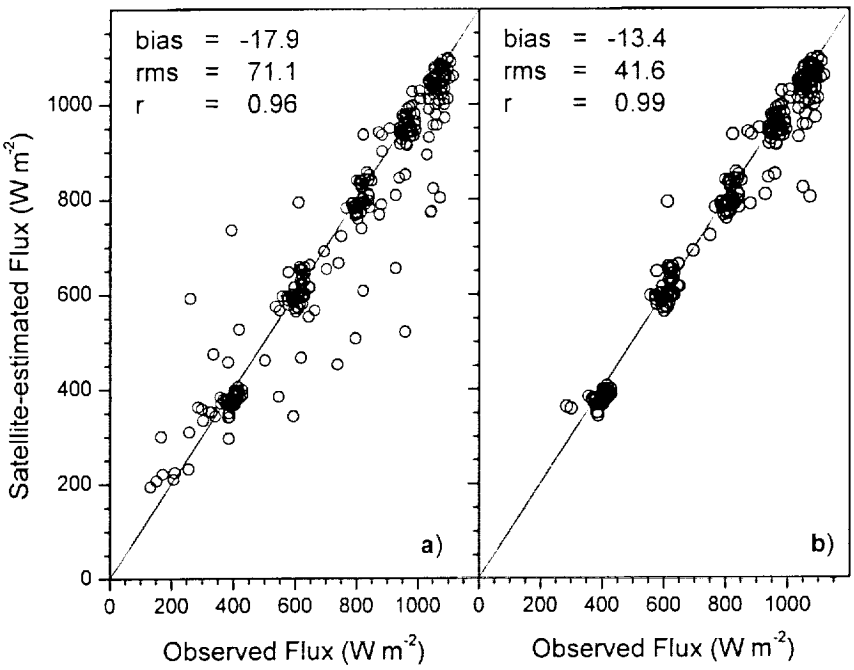
bias = -17.9
rms = 71.1
r = 0.96
a)
bias = -13.4
rms = 41.6
r = 0.99
b)
Satellite-estimated Flux (W m-2)
Observed Flux (W m-2)
Observed Flux (W m-2)
0
200
400
600
800
1000

Figure 14.

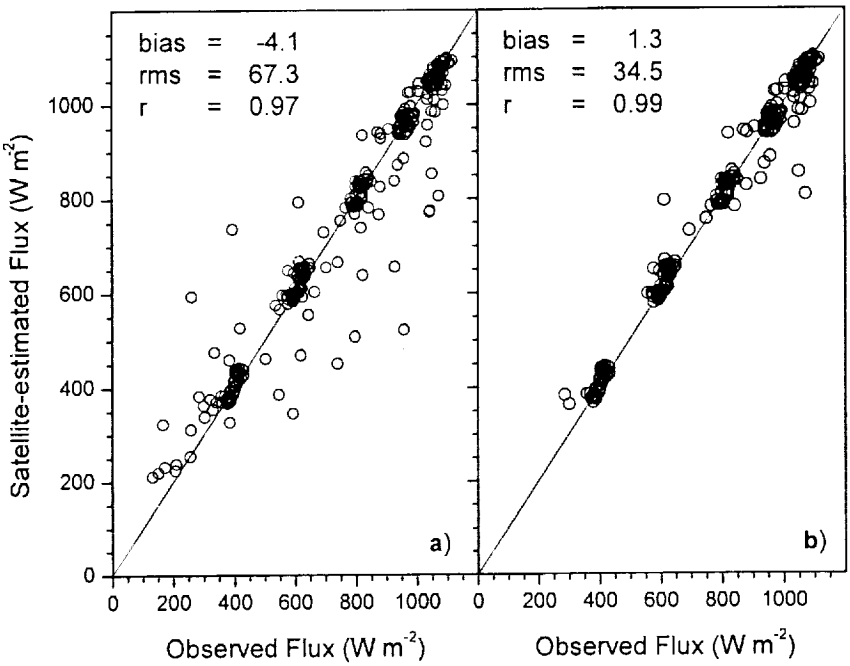
bias = -4.1
rms = 67.3
r = 0.97
a)
bias = 1.3
rms = 34.5
r = 0.99
b)
Satellite-estimated Flux (W m-2)
Observed Flux (W m-2)
Observed Flux (W m-2)
0
200
400
600
800
1000

Figure 15.